Int. J. Electrochem. Sci., 11 **(2016)** 8662 – 8682, doi: 10.20964/2016.10.47

International Journal of ELECTROCHEMICAL SCIENCE
www.electrochemsci.org

Surface Charge Storage Properties of Selected Graphene Samples in pH-neutral Aqueous Solutions of Alkali Metal Chlorides - Particularities and Universalities

Sanjin Gutić[1], *Ana S. Dobrota*[2], *Nemanja Gavrilov*[2], *Miloš Baljozović*[3], *Igor A. Pašti*[2], *Slavko V. Mentus*[2,4,*]

[1] Department of chemistry, Faculty of Science, Zmaja od Bosne 33-35, Sarajevo, Bosnia and Hercegovina
[2] University of Belgrade - Faculty of Physical Chemistry, Studentski trg 12-16, 11158 Belgrade, Serbia
[3] Laboratory for Micro and Nanotechnology, Paul Scherrer Institute, Villigen, Switzerland.
[4] Serbian Academy of Sciences and Arts, Knez Mihajlova 35, 11000 Belgrade, Serbia
[*]E-mail: slavko@ffh.bg.ac.rs

Received: 10 July 2016 / *Accepted:* 16 August 2016 / *Published:* 6 September 2016

In order to provide deeper understanding of surface charge storage mechanism in graphene materials, we analyzed the relative contribution of double layer capacitance and pseudocapacitance in overall capacitance of three different graphene-based materials in pH-neutral aqueous solutions of alkali metal chlorides. Both cyclic voltammetry at various sweep rates and DFT calculations were used for the analysis. Selected materials differ mutually to a great extent in specific surface area, surface concentration of oxygen functional groups and level of structural disorder. Measured capacitances were found to range between approx. 19 F g^{-1}, for graphene nanoplatelets, and 400 F g^{-1}, for industrial graphene. In general, measured capacitance changed directly proportionally to the cation size. Despite the differences in physical and chemical properties of graphenes subjected to investigations, similar contribution of pseudocapacitance to the overall capacitance at potentials lower than 0.4 V *vs.* Ag/AgCl was evidenced. The contribution of the pseudocapacitance increased proportionally to the concentration of oxygen functional groups. At high sweep rates, we observed the following general relationship between the capacitance retention and the fraction of pseudocapacitance: the capacitance retention is more pronounced for lower contribution of pseudocapacitance. The overall capacitive response is primarily dominated by (i) specific surface area and (ii) the concentration of oxygen functional groups. The DFT calculations revealed that the strength of the interaction of alkali metal with the oxygen functional group depends critically on the type of surface group. In order to achieve top capacitive performance of graphene-based materials one should carefully optimize the concentration of oxygen functional group so that the conductivity is not compromited while keeping specific surface area as high as possible.

Keywords: graphene, capacitance, pseudocapacitance, oxygen functional groups

1. INTRODUCTION

Preparation and investigation of carbon-based materials for application in energy storage devices, particularly in supercapacitors [1-3] and rechargeable batteries [4,5], entered into a new era with the discovery of relatively simple procedures for preparation of different graphene nanostructures [6,7]. Although theoretical surface area of graphene is as high as 2630 m^2 g^{-1}, currently available materials generally have lower values, with different moieties bounded to sp^3 hybridized carbon atoms, which can alter conductivity and electrochemical behavior of pristine graphene.

Total electrochemical capacitance of carbon-based materials can be represented as a sum of a double layer capacitance, associated with ion adsorption on solid/electrolyte boundary, and a pseudocapacitance, associated with the charge transfer across the solid/electrolyte boundary. The last one is usually associated with redox reactions of oxygen surface groups, always present to some extent on carbon material surfaces [8,9]. Electrochemical evaluation of gravimetric capacitance (expressed in F g^{-1}) is usually performed at low current densities, when galvanostatic technique is used, or at low potential sweep rates when potentiodynamic technique is used. Namely, under these conditions, all processes that may contribute to total capacitance have enough time to be completed, resulting in significantly greater values of total capacitance, compared to the ones obtained at high current densities, or high sweep rates. The capacitance retention on rising rate of charging/discharging processes is a desirable particularity of an electrochemical capacitor. Although larger surface area of different carbon materials generally leads to higher capacitance, a certain correlation was observed neither between the specific surface area and the gravimetric capacitance, nor between the specific surface area and the capacitance retention at high charge/discharge rates [1,3,10]. Main factors that affect capacitance retention at high sweep rates are pore size distribution [11-15], pore aspect ratio [16] and presence of oxygen [17-18] or nitrogen [19] functionalities, provided that final electrode material has high conductivity [9]. In a recently published computational model for equilibrium behavior of electrochemical double layer capacitors [20], the authors concluded that the relative impact of different parameters on gravimetric capacitance follows this order: specific surface area > relative permittivity of the electrolyte > hydrated ion diameter > bulk ion concentration.

Although it is known that the increase of the contribution of sp^3 hybridization in carbons leads to poorer capacitive performance, mainly due to the loss of electronic conductivity of active material [21], some recent papers [9,17-19] suggest significant increase in specific capacitance upon introduction of oxygen or nitrogen functional groups. Xu *et al*. [9] compared capacitive behavior of two materials with different oxygen content in aqueous KOH solution. They reported that specific capacitances of graphene oxide (oxygen content of 35.3 wt%, S_{BET} = 332 m^2 g^{-1}) and reduced graphene oxide (6.17 wt% O, S_{BET} = 617 m^2 g^{-1}) amount to 189 and 165 F g^{-1}, respectively. The authors concluded that redox reactions involving oxygen functionalities, especially epoxy and alkoxy ones, give rise to large pseudocapacitance, which significantly contribute to measured total values. Hsieh *et al*. [22] investigated capacitive performance of graphene oxide in aqueous Li_2SO_4 and Na_2SO_4 solutions, and reported capacitances amounted to 238.0 and 98.8 F g^{-1}, respectively. They also found that graphene oxide in Li_2SO_4 exhibits high stable capacitance, low inner resistance and high diffusivity of cations, compared to the same found in Na_2SO_4 solutions. Better performance in Li_2SO_4

solution was ascribed to lower ionic size and lower hydration number of Li^+ cation, which is a bit surprising argument. In a recently published computational study of the interactions between Li, Na and K atoms with oxygen functionalities on graphene basal plane [23], Dobrota *et al*. observed that the redox reactions of active epoxy groups are responsible for enhanced gravimetric capacitance of oxidized graphene, in agreement with the experimental observations [9]. It was also found that the interactions of alkali metals with hydroxyl groups could lead to irreversible reduction of graphene oxide and formation of corresponding hydroxide, which was surprising results considering recent experimental results on reversible interaction of OH groups with Li^+ ions [5]. This discrepancy was explained showing that OH groups are stabilized by agglomeration over basal plane and can take part in surface faradaic processes [24].

While commercial electrochemical capacitors typically employ activated carbons and non-aqueous electrolytes to achieve higher energy densities, enabled by wider operating voltage [25], electrochemical capacitors with aqueous electrolytes are more attractive thanks to a lower price and simpler production procedures. However, typical carbon materials enable relatively narrow potential window in aqueous media [26], which can be expanded using pH-neutral aqueous solutions [27,28]. For this reason, we investigated in this study capacitive performance of three different commercial graphene-based materials, different in structures, oxygen contents and surface areas, using cyclic voltammetry in neutral aqueous lithium, sodium, and potassium chloride. We analyzed the effects of both electrolyte composition and graphene properties on the capacitance. Experimental measurements were supplemented by theoretical Density Functional Theory (DFT) calculations.

2. EXPERIMENTAL

2.1. Materials and chemicals

Three commercially available ACS products [29] were selected for the present study: Graphene Oxide Powder (GO, [30]), Industrial-Quality Graphene (IG, [31]), and Graphene Nanoplatelets (GNP, [32]). All the chemicals were of analytical grade and all solutions were prepared with doubly-distilled water. Lithium chloride, sodium chloride, potassium chloride and ethanol were obtained from Sigma-Aldrich and used as received. Vulcan XC-72 R was obtained from Carbot (USA), while 5% ethanol solution of Nafion was obtained from Alfa Aesar.

2.2. Materials characterization

Raman spectra, excited with a HeNe gas laser (excitation wavelength 633 nm), were collected on a DXR Raman microscope (Thermo Scientific, USA) equipped with an Olympus optical microscope and a CCD detector. The laser beam was focused on the sample using objective magnification 50×. The scattered light was analyzed by the spectrograph with a 900 lines mm^{-1} grating. Laser power on the sample was kept at 1 mW.

Graphene samples were characterized at room temperature by X-ray powder diffraction (XRD) using Ultima IV Rigaku diffractometer, equipped with Cu Kα1,2 radiation source, using a generator voltage of 40.0 kV and a generator current of 40.0 mA. The range of 3–90° 2θ was used for all powders in a continuous scan mode with a scanning step size of 0.02° and at a scan rate of 2° min^{-1}.

XPS spectra were collected using SPECS Analyzer Phoibos 150, with monochromatic AlK_{α} source (energy of 1486.6 eV, power 400W). The base pressure in the spectrometer was 10^{-11} mbar. Data acquisition was controlled using SpecsLab2 software, while analysis was done using Unifit2013 software and its sensitivity factors database.

2.3. Electrochemical measurements

Cyclic voltammetry measurements were performed in a three-electrode electrochemical cell, with Ag/AgCl (saturated KCl, 0.197 V *vs*. SHE at 25°C) as a reference and platinum foil as a counter electrode. Voltammetric response was recorded with Princeton Applied Research 263A potentiostat/galvanostat, controlled by PowerCV software. Working electrode was prepared by direct drop casting of active material suspension on a pre-cleaned glassy carbon disc and subsequent drying under the vacuum. The suspension was obtained by dispersing each of the graphene sample in ethanol/water mixture (40 v/v%), and homogenizing the suspension in an ultrasonic bath for 30 min. Nafion solution and Vulcan XC-72R were also added to the suspension. Nafion was added to the final concentration of 0.05% in order to improve the adhesion of the active layer to the surface of the glassy carbon disk and the integrity of the thin film during the electrochemical testing. Vulcan XC72-R (added to the concentration of 10 wt.%) was used to average differences in the conductivity of thin films of active material [33] and to prevent stacking and agglomeration of graphene sheets during the drying on the glassy carbon surface [34]. The electrochemical cell was degassed under vacuum, in order to remove oxygen sorbed in the active material films, and purged by blowing argon prior and during the measurements. Values for gravimetric capacitances were calculated according to the equation [35]:

$$C = \frac{Q}{2 \cdot \Delta V \cdot m} = \frac{\int i \mathrm{d}t}{2 \cdot \Delta V \cdot m} \qquad (1)$$

where C is gravimetric capacitance in (F g^{-1}), Q is the voltammetric charge obtained by integration of positive and negative sweep in cyclic voltammograms, ΔV is the width of the potential window and m is the mass of the active material loaded on the glassy carbon electrode surface.

2.4. Theoretical calculations

In order to provide deeper insight into the role of oxygen functional groups in surface faradaic processes that contribute to the overall capacitance, we have analyzed the interactions of alkali metal atoms with several types of oxygen functional groups using DFT calculation. The presence of solvent was excluded in the calculations, but as explained previously [23] the final charge distribution does not differ from that observed in electrochemical system where electron comes from the external electrical circuit and the ion comes from the electrolytic solution. The DFT calculations were performed within the generalized gradient approximation (GGA) and Perdew–Burke–Ernzerhof (PBE) exchange correlation functional [36] using ultrasoft pseudopotentials implemented in the PWscf code of the Quantum ESPRESSO distribution [37]. The spin polarized formalism was used in all calculations. The plane waves' kinetic energy cutoff was 36 Ry, while the charge density cutoff was 576 Ry. Pristine graphene (*p*-graphene) was modeled as a 24 carbon atoms layer (C_{24}) within a hexagonal supercell, while graphene with a monovacancy (*v*-graphene) was obtained by simply removing one C atom from the carbon plane (C_{23}) and relaxing the structure. Oxygen functional groups were introduced on the graphene basal plane. The first irreducible Brillouin zone was sampled using a Γ-centered 4×4×1 grid of *k*-points generated by the general Monkhorst-Pack scheme [38]. The convergence with respect to the vacuum layer thickness and the *k*-point mesh was confirmed. Atomic positions were fully relaxed until the residual forces acting on atoms became smaller than 0.002 eV $Å^{-1}$. The charge analysis was done using the Bader algorithm [39] on a charge density grid by Henkelman *et al.* [40].

The interactions of chosen alkali metal atoms (M) with pristine and oxygen-functionalized graphene surfaces was quantified in terms of adsorption energies (E_{ads}(M)), defined as:

$$E_{\mathrm{ads}}(\mathrm{M}) = E_{\mathrm{subs+M}} - (E_{\mathrm{subs}} + E_{\mathrm{M}}) \qquad (2)$$

where $E_{\mathrm{subs+M}}$, E_{subs} and E_{A} denote the total energy of the substrate with M adsorbed, the total energy of the bare substrate, and that of isolated atom M. Dispersion interactions were included using semiempirical DFT-D2 approach [41].

3. RESULTS AND DISCUSSION

3.1. Characterization of materials

For the present study we have chosen commercial graphene samples with versatile physical and chemical properties, aiming to link these properties to the capacitive behavior in the pH-neutral alkali metal chloride solutions. Some of the properties of used materials are provide by manufacturer (Table 1), while additional characterization was performed using Raman spectroscopy, XRD and XPS.

Table 1. Physical properties of selected graphene samples provided by manufacturer (SSA stands for specific surface area).

Sample	SSA / $m^2\ g^{-1}$	Thickness / nm	Diameter / µm	Conductivity / S cm^{-1}
GO	5-10	0.8-1.2	1-15	-
IG	~600[a]	≤3.0	>0.5[b]	> 3
GNP	20-40	2-10	~5	800

[a]given as S_{BET} [31], [b]based on SEM and TEM images [31]

Besides the data provided in Table 1, XRD patterns (Fig. 1), Raman spectra (Fig. 2) and XPS spectra (Fig. 3), also point that selected materials have rather different properties. XRD pattern of graphene-oxide is characterized by intensive reflection at 2θ = 11.8° indicating much larger distance between graphene-oxide sheets (around 8 Å) compared to those of graphite. This is due to the appearance of oxygen functional groups over GO basal plane which increases the distance between graphene sheets and is typical feature of graphene-oxide [42,43]. XRD pattern of IG sample (Fig. 1, middle) does not show any particular features except rather weak and diffuse (002) graphite reflection around 2θ = 25°. The GNP sample displayed typical XRD pattern of graphite with sharp (002) reflection at 2θ = 26.4° and (004) reflection at 2θ = 54.4° [43].

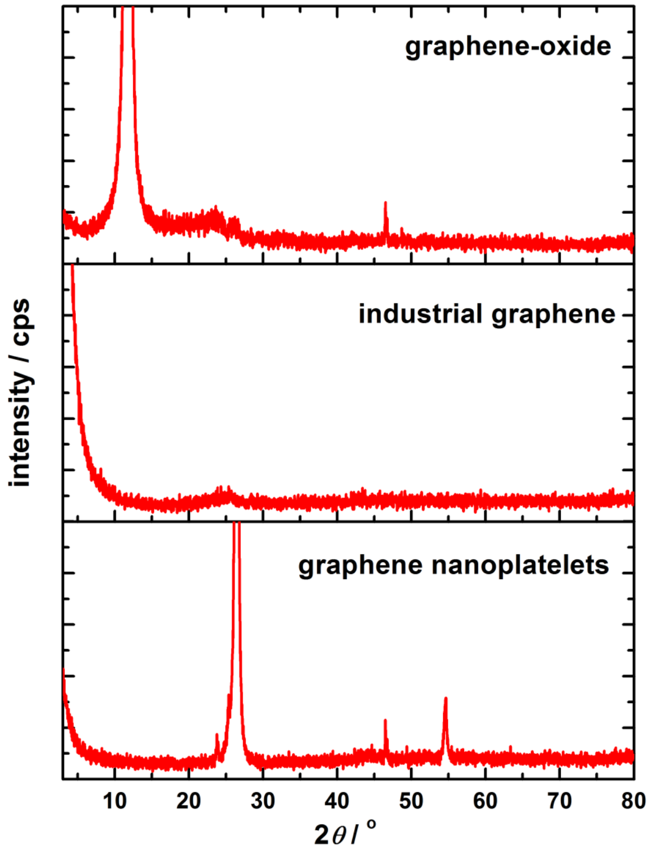

Figure 1. XRD patterns of selected graphene materials

Although the analysis of Raman spectra can provide much information here we focus on the structural disorder of the samples which can be accessed from the analysis of G-band, located around 1580 cm^{-1}, and D-band, located around 1350 cm^{-1}) [44]. It can be seen that the structural disorder decreases going from GO to IG and GNP, where D-band is completely absent (Fig. 2). This correlates well with the relative contribution of sp^2 hybridized carbon in C 1s XPS spectra of these materials (not shown here). Namely, the relative contribution of the sp^2 hybridized carbon was found to be 20%, 60% and 66% for GO, IG and GNP samples, respectively. This clearly indicates that the level of preservation of original π electronic system of graphene layer increases in the same order, which is also in agreement with the relative differences in the conductivities of IG and GNP (Table 1).

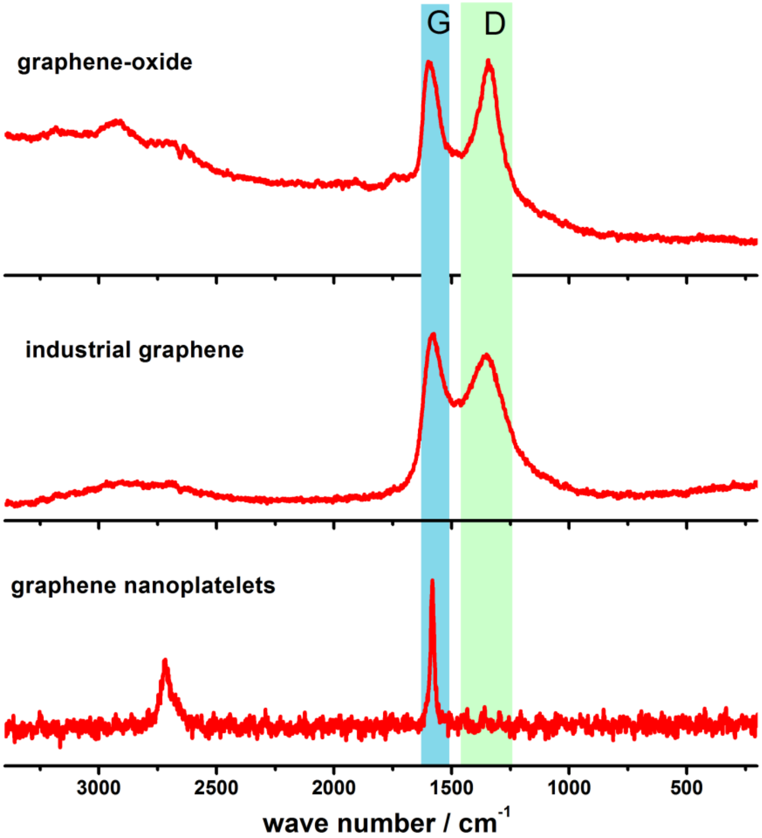

Figure 2. Raman spectra of selected graphene materials

The analysis of XPS spectra, in general, revealed that the selected materials differ in the concentration of oxygen functional groups, while small amount of nitrogen was also found in the GO sample (Table 2).

Table 2. Elemental composition of selected graphene materials determined by XPS analysis

Sample	C / at.%	O / at.%	N / at.%
Graphene-oxide	70.60	28.54	0.87
Industrial graphene	94.10	5.90	-
Graphene nanoplatelets	98.76	1.24	-

The additional analysis of the high resolution O 1s signals of selected materials (Fig. 3) also revealed a variety of presented oxygen functional groups. Following some of previously reported research [24, 45-47], we have concluded that the GNP sample contains dominantly OH groups attached to C atoms at the edge sites, while IG contains OH groups distributed over basal plane with carbonyl functions at edge sites. Graphene-oxide analyzed here contains different oxygen functional groups, located at both edge and basal plane sites (hydroxyl, phenol, epoxy, carbonyl and carboxyl groups). Based on the performed analysis we consider that the described materials are characteristic of hydrophobic surface (preserved sp^2 hybridized basal plane) with hydrophilic, oxygen-rich areas. This model is plausible, as there are theoretical [24,48] and experimental [49] evidences of the stabilization of the oxygen-functionalized graphene through aggregation of chemisorbed oxygen groups on its surface. As mentioned above, edge sites can also contain oxygen functional groups and present the sites of enhanced reactivity [17,50].

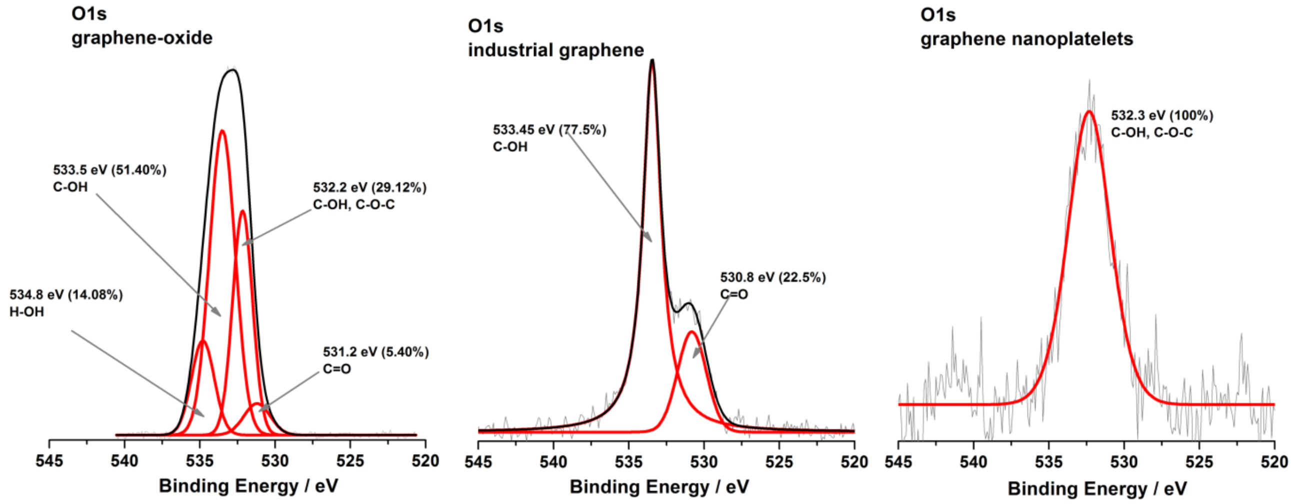

Figure 3. De-convoluted high resolution O 1s XPS spectra of selected graphene materials (assignation and relative contribution of each oxygen functional group is included in the figure). Note that the intensities of signals are different for each presented spectra.

3.2. Capacitive performance

In order analyze the role of physical and chemical properties of graphene samples and the type of electrolyte on the capacitive behavior, all three materials were investigated by cyclic voltammetry in 1 mol dm^{-3} aqueous solutions of LiCl, NaCl and KCl. The first observation was that the potential window available for these measurements depends on the type of the material. In the case of IG and GNP capacitive currents were recorded between −1.0 and 0.8 V *vs*. Ag/AgCl electrode while for the case of GO this window is reduced to −0.5 to 0.8 V *vs*. Ag/AgCl electrode. In the case of graphene-oxide, much narrower potential window is available for recording capacitive currents (Fig. 4), since surface structure is able to change by the irreversible reduction of GO. This issue will be discussed in more details later on. Regardless of their different physical and chemical properties, all three materials share some common voltammetric features: (i) lower capacitive response at the potentials above 0.4 V, (ii) increase of cathodic currents at 0.4 V with the emergence of broad pseudocapacitive peak between 0.4 and 0.1 V and (iii) higher capacitive currents at potentials below 0.1 V. At more negative potentials, current responses for all three materials increase when electrolyte cation is changed in the order $Li^+ \rightarrow Na^+ \rightarrow K^+$, whereby this trend is more pronounced for anodic currents (Fig. 4). Voltammograms for IG and GNP do not show significant deviations from rectangular shape, in contrast to GO, for which significant deviation from ideal capacitive behavior is evident at negative potentials. For all three materials, rectangular shape is best preserved in aqueous KCl. The trends observed for different electrolytes are more pronounced at higher scan rates. The here described measurements indicated that available potential windows are separable to the regions where either double layer capacitance or pseudocapacitance dominate.

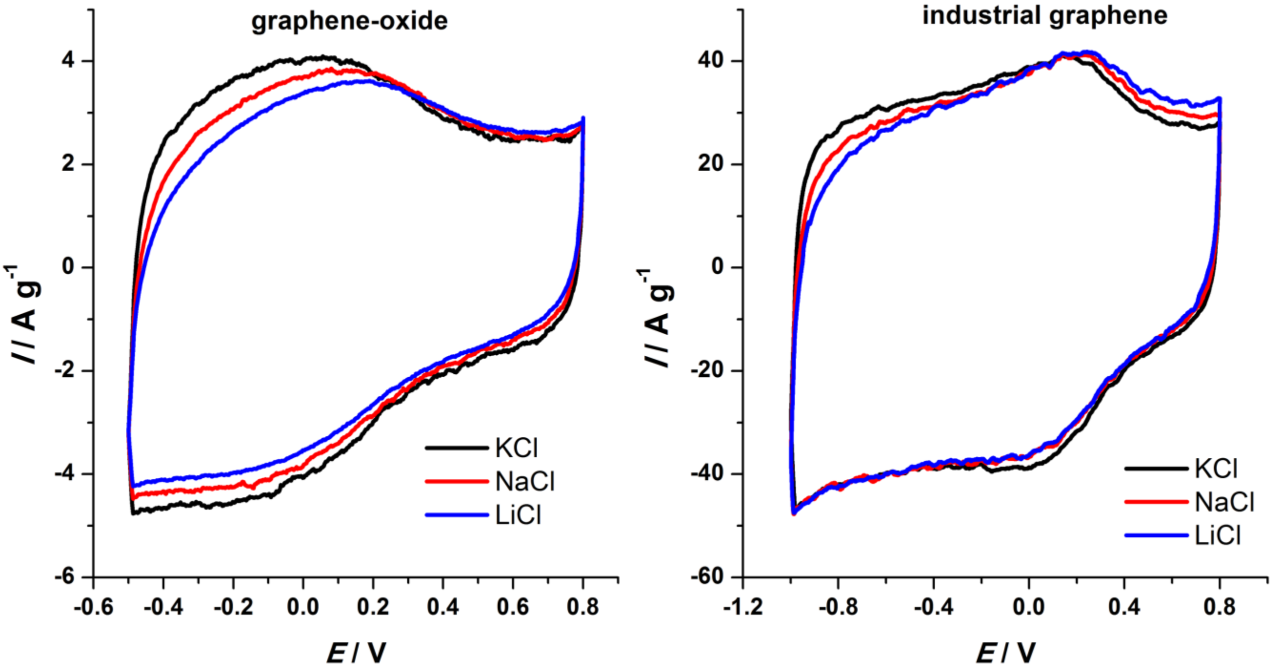

Figure 4. Cyclic voltammograms of graphene-oxide (left) and industrial graphene (right) recorded at 100 mV s^{-1} in 1 mol dm^{-3} aqueous solutions of LiCl, NaCl and KCl. Vertex cathodic potential in the case of graphene-oxide is limited by onset potential of the irreversible reduction of this material.

For more detailed analysis of the observed trends, cyclic voltammetry measurements of all three materials in three different electrolytes were performed in two distinct potential windows: (i) between 0.4 V and 0.8 V, denoted here as double layer (DL) region, and between vertex cathodic potential (−1.0 V for IG and GNP; −0.5 V for GO) and 0.4 V (denoted here as pseudocapacitive region). Measurements were performed at scan rates between 15 and 800 mV s^{-1}. Obtained cyclic voltammograms indicate pronounced increase of capacitive currents as the electrolyte cation is changed from Li^+ to K^+ in pseudocapacitive region, while the same trend is present but much less prominent in DL ragion (Fig. 5). Further, in the pseudocapacitive region rectangular shape of voltammograms is improved on going from Li^+ to K^+, indicating better capacitive behavior, i.e., faster charge/discharge processes. Since the observed effects were more pronounced only in pseudocapacitive range and one of the aims of this work is to evaluate the effects of the cation type on the capacitive behavior, further discussion is focused on the measurements obtained in the pseudocapacitive region.

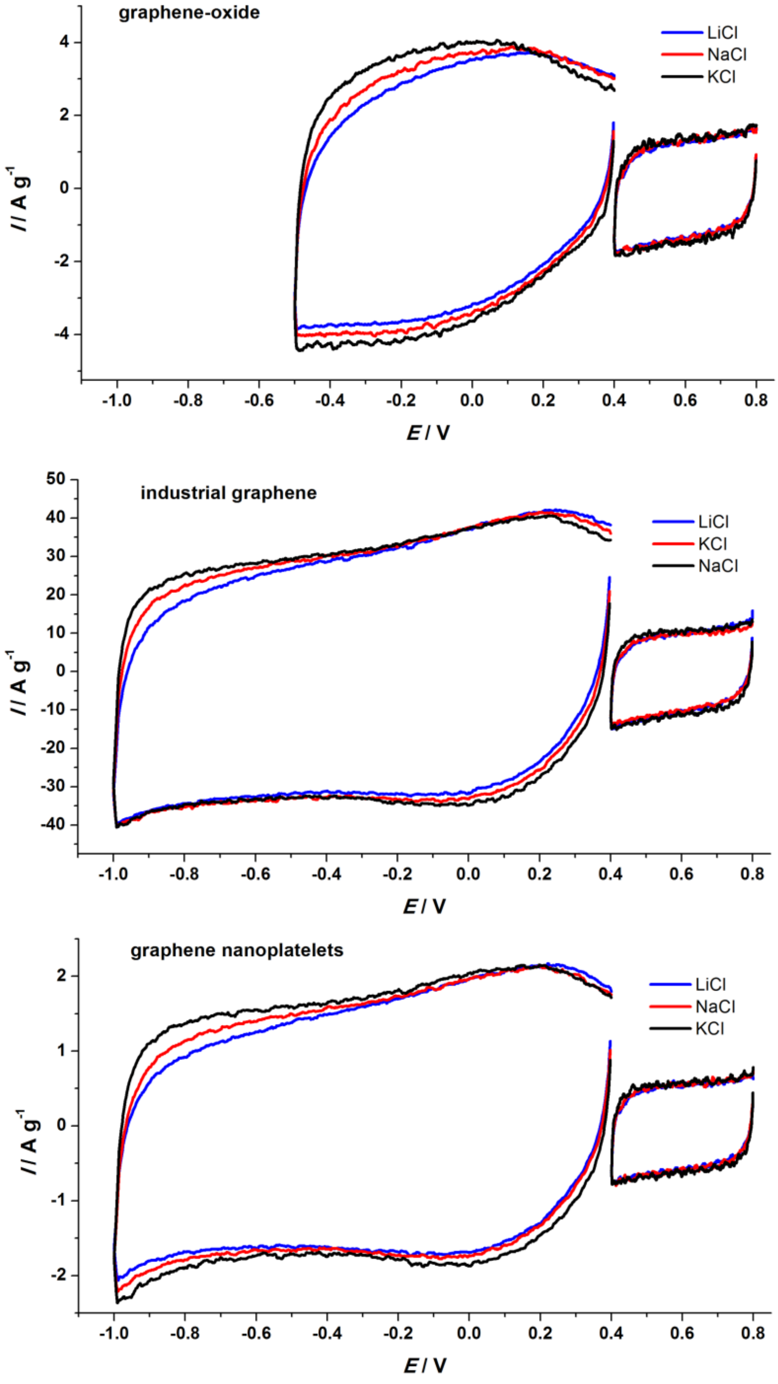

Figure 5. Cyclic voltammograms of graphene-oxide (top), industrial graphene (middle) and graphene nanoplatelets (bottom) recorded at 100 mV s^{-1} within two different potential windows in 1 mol dm^{-3} aqueous solutions of LiCl, NaCl and KCl.

It is well established that materials’ capacitances decrease with the increase of scan rate (current load). This is due to the fact that at high scan rates (or high current densities) slow processes involving faradaic reactions and adsorption in micropores, contributing significantly to the capacitance, are unable to finalize. This behavior was confirmed for all three materials investigated here (Fig. 6).

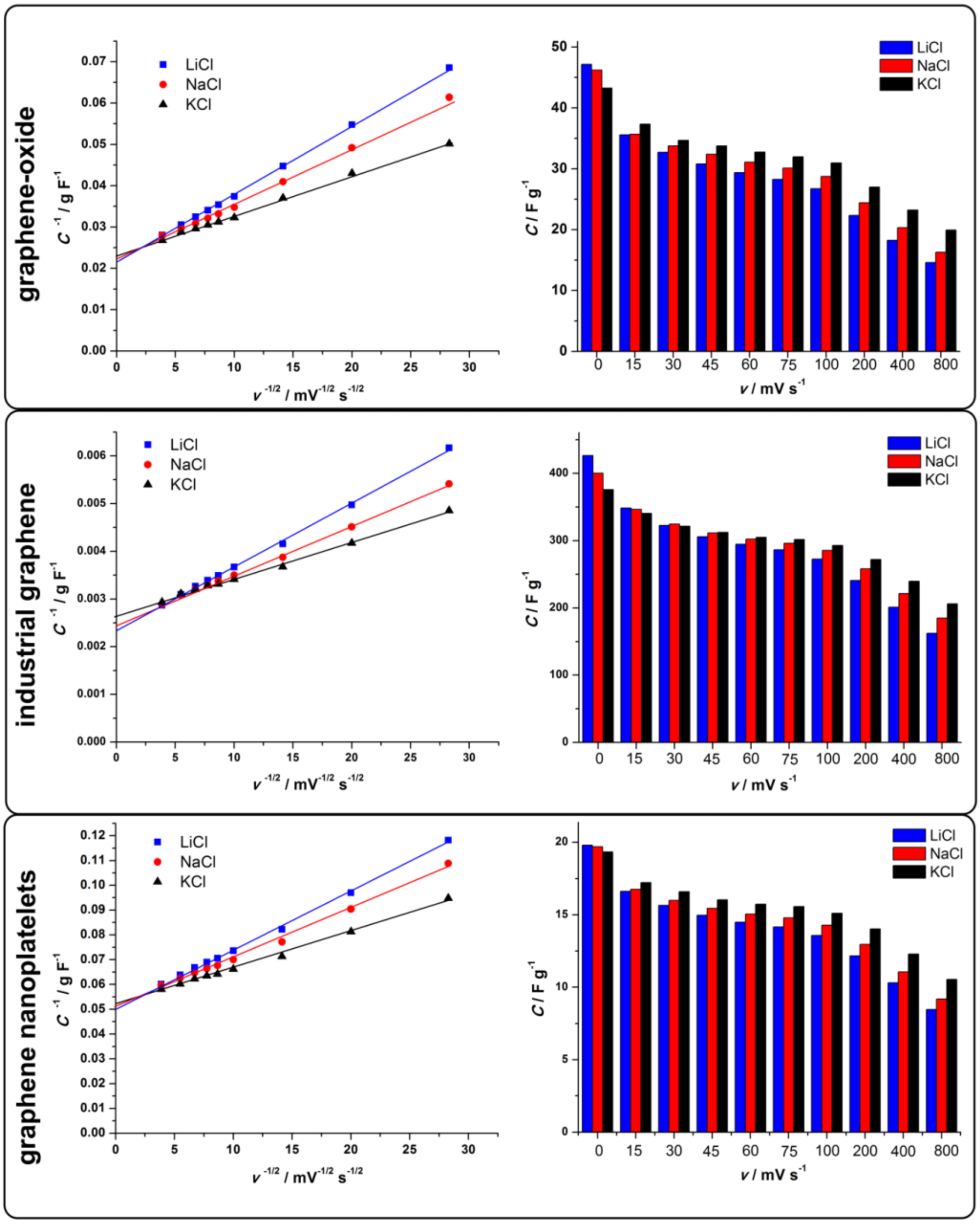

Figure 6. Left: $1/C$ vs. $v^{1/2}$ function for three investigated materials, right: measured values of gravimetric capacitance (in F g^{-1}) in 1 mol dm^{-3} aqueous solutions of LiCl, NaCl and KCl at the potential scan rates between 15 and 800 mV s^{-1}.

More detailed analysis can be performed further by following ref. [19] where it was shown that linear dependence between $1/C$ and $v^{1/2}$ can be obtained for a broad range of potential scan rates.

Extrapolation of this function to $v = 0$ mV s^{-1} gives the limiting value of the capacitance that could be obtained at infinitely low scan rate and includes both DL charging and pseudocapacitive processes. All three investigated materials show linear dependence, for scan rates in the range from 15 to 800 mV s^{-1} (Fig. 6), allowing for accurate extrapolation to $v = 0$ mV s^{-1}.

Considering the overall features of the effects of the type of the electrolyte, two distinct trends for capacitance values can be observed, depending on scan rate: (i) the decrease of the gravimetric capacitance on going from LiCl to KCl at lower scan rates ($v \rightarrow 0$) and (ii) the increase of the specific capacitance on going from LiCl to KCl at higher potential scan rates (Fig. 6). It is evident that, for all three materials, extrapolated values ($v = 0$ mV s^{-1}) are the highest when measured in LiCl (Fig. 6, Table 2), but the observed trend inverts at realistic scan rates. Namely, for $v > 45$ mV s^{-1} measured capacitances increase as the cation is changed from Li^+ to Na^+ and K^+. Moreover, capacitance for GO and GNP increase from LiCl to KCl for all applied scan rates. The IG sample shows similar behavior, except that the change of the trend is slightly delayed, i.e. the trend observed at lower scan rates is same as for $v = 0$ mV s^{-1}, and gradual inversion with the increase of the scan rate can be clearly observed (Fig. 6, right). It should be emphasized that the differences between measured capacitances in different electrolytes are the most pronounced at high scan rates, and this is observable for all three materials.

Besides the similarities in the overall trends, three considered materials displayed very different capacitances. The values recorded at 15 and 800 mV s^{-1} and the ones obtained upon the extrapolation to $v = 0$ mV s^{-1} (Table 2) show that the lowest capacitance is provided by GNP, followed by GO, while the highest capacitance has IG, reaching rather high values of around 400 F g^{-1} at low scan rates. The value of several tens of F g^{-1} measured for GO and GNP are comparable to capacitances of graphite electrodes [51]. The capacitances measured for IG are similar to some other carbons reported in the literature but still rather high [46,52,53]. Moreover, the connection between measured capacitances and the specific surface areas of investigated materials suggests that high specific surface area is crucial for achieving high gravimetric capacitances, in agreement with the ref. [20].

Table 2. Measured capacitance at low (15 mV s^{-1}, C_{15}) and high scan rate (800 mV s^{-1}, C_{800}) for three investigated materials in 1 mol dm^{-3} aqueous solutions of LiCl, NaCl and KCl. The value obtained by extrapolation to 0 mV s^{-1} ($C_{v\rightarrow 0}$) is included. Capacitance retention was calculated comparing the values measured at 800 mV s^{-1}, with the values obtained after extrapolation to $v = 0$ mV s^{-1} as a reference.

	$C_{v\rightarrow 0}$ / F g^{-1}			C_{15} / F g^{-1}			C_{800} / F g^{-1}			Capacitance retention / %		
	LiCl	NaCl	KCl	LiCl	NaCl	KCl	LiCl	NaCl	KCl	LiCl	NaCl	KCl
GO	47.2	46.2	43.3	35.6	35.7	37.3	14.6	16.3	19.9	30.93	35.28	45.96
IG	426.5	400.3	376.0	348.5	346.3	340.6	162.0	184.7	205.9	37.98	46.14	54.76
GNP	19.8	19.7	19.3	16.6	16.8	17.2	8.46	9.19	10.54	42.73	46.67	54.50

As regards to the measured gravimetric capacitances, the values of both GNP and GO are rather small. In order to obtain better insight into the effects of physico-chemical properties of these materials on the measured capacitance, one can evaluate capacitance *per* unit of real surface area. Taking the average capacitance values obtained upon the extrapolation to $v = 0$ mV s^{-1} ($C_{v\rightarrow0}$, Table 2) for each material and in all three electrolytes, and the value of specific surface area of these materials (upper limits of the reported SSA, Table 1), one obtains the values of 450, 67 and 49 µF cm^{-2}. These values significantly deviate from the value of 20 µF cm^{-2} which is taken as a typical DL capacitance of smooth carbon surface [54]. This indicates that the contribution of the pseudocapacitance is extremely high in all cases, but, more importantly, it decreases in the same manner as the amount of oxygen functional groups and the structural disorder in the samples. Hence, in order to achieve high values of capacitance *per* real surface area unit, significant concentration of functional groups that can provide redox reactions is necessary. Considering that surface redox processes are much slower than DL charging processes one would expect, in general, that the capacitance retention is higher when the contribution of the pseudocapacitance processes is lower, which is indeed obtained here (Table 2). This relationship and the effect of the type of the cation on the capacitance are elaborated below.

Following ref. [55], three general types of processes can be distinguished during cathodic polarization in acidic electrolyte:

(i) physical, nonspecific adsorption by electrostatic forces between carbon surface and proton:

$$>C_x + H^+ \rightarrow C_x//H^+ \qquad (3)$$

(ii) specific, ion-dipole interaction between proton and quinone- or carbonyl-type groups:

$$>C_xO + H^+ \rightarrow C_xO//H^+ \qquad (4)$$

(iii) reversible formation of strong bond due to the electron transfer, i.e. faradaic reaction responsible for pseudocapacitance:

$$>C_xO + H^+ + e^- \rightarrow C_xOH \qquad (5)$$

These processes can be considered in pH-neutral aqueous electrolyte as well, except that a complex is formed with M^+ ion (here alkali metal ion). Specifically, faradaic reaction (5) would result in an ionic complex, $>C_xO^-M^+$, as reduction of alkali metal ion is not possible in aqueous media. However, this scenario is possible only if an oxygen group can be stabilized in the anionic form upon the reduction. While processes (3) and (4) are possible in the entire potential window, reaction (5) can be expected only at sufficiently low cathodic potentials. This agrees with our observation that pseudocapacitance rise is triggered at low potentials (Fig. 5).

Several different phenomena should be taken into consideration when discussing capacitive behavior [20]. Although there are some differences in values stated in literature, it is generally accepted that dimensions of total hydration spheres, as well as interaction energies between alkali metal cation and water decrease significantly in cation series from Li^+ to K^+ [56,57]. Because of its highest charge density, total hydration number (including strongly bound second hydration sphere) of lithium ion is higher than that of sodium ion [12,57], while hydration sphere of potassium ions consist only of first-layer water molecules, interacting directly with cation. Considering that nonspecific adsorption, reaction (3), is based on weak dispersion interactions, and that oxygen-free surface is hydrophobic, adsorption energy only is not sufficient to compensate for the dehydration of lithium ions or to induce significant changes in solvation environment, thus making hydrated lithium species adsorbed in this manner to be the largest. This implies that, in aqueous solution, double-layer capacity should have the smallest value for lithium cation, as it occupies the largest volume due to its hydration sphere. Similar conclusions might be derived for the reaction (4), although much higher adsorption energies can be expected when solvated alkali metal ion interacts with oxygen functional group, as these bear partial negative charge [23,24,58].

Considering the reaction (5), much stronger interactions are expected, and oxygen functional groups (and other types of defects) play a crucial role here. We have recently studied the effects of oxygen functional groups (epoxy and hydroxyl) on alkali metal ion storage capabilities of graphene [23,24]. Alkali metal atoms transfer their charge completely to oxygen-functionalized graphene, indicating ionic type of interaction, but the type of oxygen functional group may lead to certain differences. In principle, single epoxy-group over graphene basal plane can accept electron from alkali metal atom and allow the formation of stable complex, which does not hold for the case of an isolated OH groups [23,58]. In general, clustering of hydroxyl groups in certain configurations prevents formation of metal hydroxide or water, i.e., the reduction of OH-functionalized graphene, making the interaction between metal ion and graphene substrate reversible at negative potentials [24]. On the basis of calculated both interaction energies and charge distribution, we concluded that strength of interaction between alkali metal atoms and hydroxylated domains should increase on going from Li to K, which implies that the gravimetric capacitance will follow this trend in the case of graphene dominantly functionalized by OH groups [24]. Here we complement previously reported theoretical results to emphasize the effects of oxygen functional groups in enhancing capacitance through the faradaic reactions. We have analyzed the interactions of Li, Na and K with epoxy-functionalized graphene and found that the strength of the interaction increases in the order Na < K < Li, and the $E_{\mathrm{ads}}(\mathrm{M})$ were −0.82 eV, −1.05 eV and −1.79 eV. These adsorption energies are significantly more exothermic compared to the case of the adsorption of alkali metals on pristine graphene [23]. In addition to the effect of the type of the cation, the nature of oxygen-functional group also plays important role, as demonstrated here for the case of the Na interaction with different types of graphene surfaces (pristine graphene, epoxy-graphene, carboxyl-graphene and graphene with monovacancy, the later one was selected as a representative of structurally disordered graphene). Adsorption energies range between −0.35 eV to less than −2 (Fig. 7). Dispersion interactions contribute to the adsorption by stabilization for 0.3 to 0.4 eV. Bader analysis showed that almost in all cases valence s electron from alkali metal is completely transferred to oxygen functional group (defect) on graphene surface. This confirms formation of strong ionic complex, $>C_xO^-M^+$ (O stands here for different type of oxygen moieties present in investigated materials). Additional sites where strong interaction can take place are certainly the edge sites [50,59] and we expect that they contribute significantly to the capacitance of graphene nanoplatelets (GNP sample) investigated here. Due to the applied methodology, solvation energies were not included in the calculations but we expect that stronger salvation hinders the interaction of cations with O-functional groups to greater extent, so that this effect is being the most prominent in the case of Li^+ and the least prominent in the case of K^+. This stands in favor of our observation that typically gravimetric capacitance decreases as the electrolyte changes from KCl to LiCl.

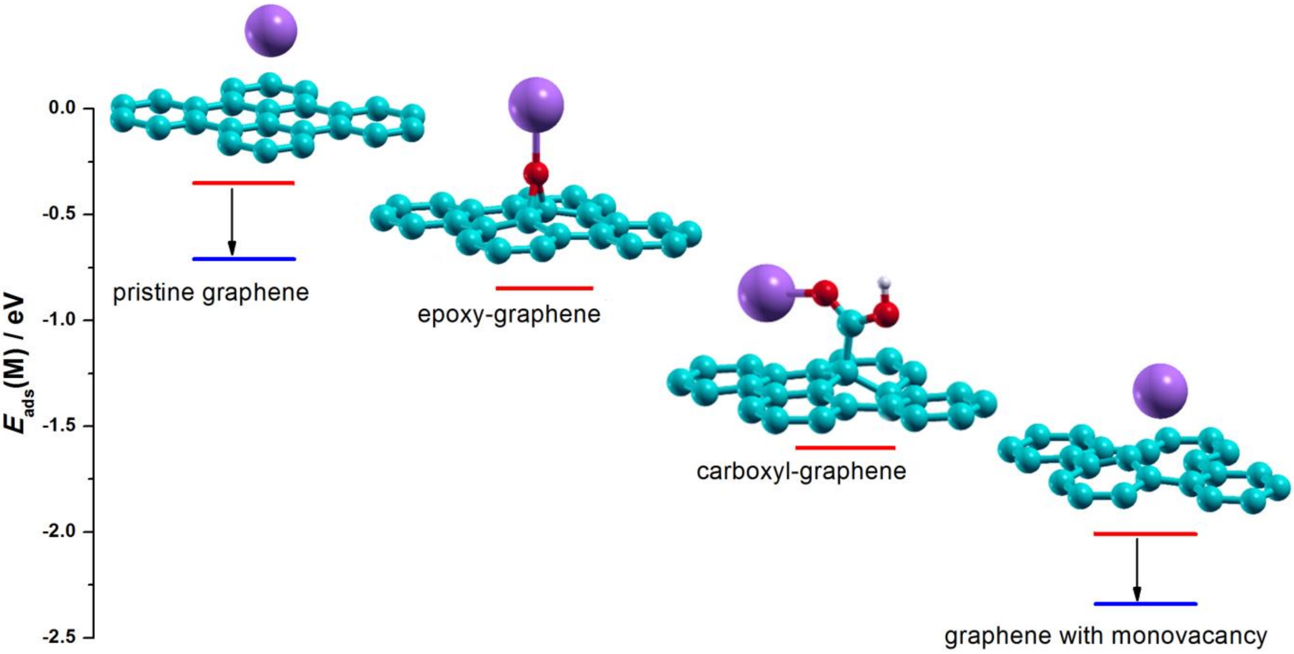

Figure 7. Calculated adsorption energies of Na on pristine graphene, epoxy-graphene, carboxyl-graphene and graphene with monovacancy. Vertical arrows indicate the contribution of dispersion interactions on E_{ads}(Na).

To summarize that said so far, both experimental and theoretical results indicate that the formation of a strong bond between metal cation and reduced form of oxygen functional group on graphene surface (due to the faradaic reaction responsible for pseudocapacitance) is obviously highly sensitive to the type of the oxygen functionality (or other types of defects which can participate in this process) and the type of cation present in the electrolytic solution. However, the question is whether some general observation regarding the capacitive behavior can be derived for such diverse materials as are the ones used in this work?

As done previously, the intercept of the linear function of $C^{-1} = f(v^{1/2})$ gives the values of capacitance that can be interpreted as the total capacitance, arising from both fast and slow processes taking place during the potentiodynamic cycling [19]. The same authors proposed that this dependence can also be used to calculate exact contributions of double-layer and pseudocapacitance to the total capacitance. This is done by rearranging the function to the form $C = f(v^{-1/2})$ and extrapolating its linear part to $v \to \infty$ mV s^{-1} (i.e. $v^{-1/2} = 0$), which should give the value of pure double-layer capacitance (i.e., the capacitance arising from the fast processes that can occur at $v \to \infty$) [19]. This method was applied to our data in the same manner, and gave surprisingly high values of what would be described as pseudocapacitance according to ref. [19]. Namely, for all three materials these values are found to range between 25 and 50 % and were found to decrease on going from LiCl to KCl. The highest percentage of pseudocapacitance was found for the case of GO which has the highest concentration of oxygen-functional groups and the lowest one was observed for GNP (Fig. 8). Although the values of capacitance calculated *per* real surface area unit (which decrease in the same manner as the concentration of oxygen functional groups) would indeed point to high contribution of pseudocapacitance, possible explanation for such a high value can be given if not only faradaic reactions, but also some other slow processes contribute to measured capacitance at low scan rates [11]. This could possibly be diffusion of cations which is faster for K^+ compared to Li^+ due to lower hydratation number. This would also explain why the percentage of pseudocapacitance decreases from LiCl to KCl. In addition, a linear relationship between capacitance retention at high potential scan rates (Table 2) and the percentage of pseudocapacitance was observed for all materials (Fig. 8). Moreover, the data points for all three material fall on the same line, suggesting a general conclusion that the capacitance fade at high current loads will be lower if the contribution of faradaic processes to the overall capacitance is lower. This also excludes the effects of the specific surface area on the capacitance retention.

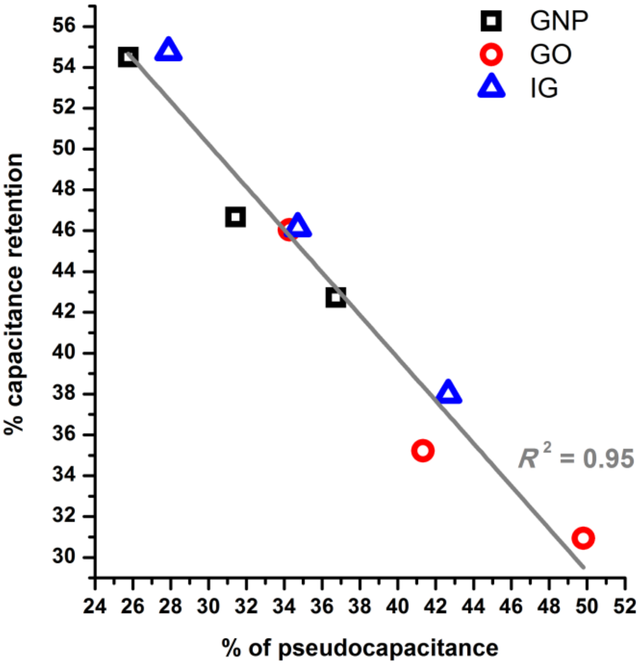

Figure 8. Capacitance retention at 800 mV s^{-1} as a function of percentage of pseudocapacitance for investigated materials. Highest capacitance retention (thereby, the lowest fraction of pseudocapacitance) for all three materials were obtained in KCl, followed by NaCl and LiCl.

3.3. Some additional electrochemical features of graphene oxide

While graphene-oxide does not allow potential cycling in wide potential window, which is undesirable from the aspect of practical application, this material displayed two additional phenomena related to the capacitive behavior that were not observed in the other two cases, i.e., IG and GNP samples. These two phenomena are (i) tunable capacitance upon electrochemical reduction at potentials below −0.5 V vs. Ag/AgCl and (ii) “activation” of material upon prolonged cycling which is dependent on the type of the cation present in solution.

As mentioned previously, vertex cathodic potential to which graphene-oxide shows reversible capacitive behavior is not lower than −0.5 V *vs*. Ag/AgCl in pH-neutral solutions. Upon deeper cathodic polarizations irreversible reduction of GO takes place (Fig. 9) which is well known feature of inherent oxygen functionalities present in graphene-oxide [56]. Irreversible changes caused by reduction of grapheme oxide at potentials lower than -0.5 V have interesting effect on the capacitance measured within a constant potential window between −0.5 and 0.8 V vs. Ag/AgCl. Namely significantly higher values passing the maximum are found after reduction at various potentials. The values increased for maximum 60% (Fig. 9) above its reversible initial value, when GO is polarized to moderate cathodic potentials (−1 V *vs*. Ag/AgCl), but decay up to 40% above its reversible value if the reduction potential is further extended to -1.5 V(Fig. 9). While a definite explanation of such behavior is still to be provided, we suggest that the reason of this behavior is a fine interplay of two different processes: (i) removal of oxygen functional groups upon the reduction of graphene oxide [60] and (ii) increase of conductivity due to the restoration of the delocalized π electronic system [61]. According to ref. [60], continuous removal of oxygen-functional groups is taking place upon graphene-oxide is subjected to deeper cathodic polarization. In the same manner the conductivity is being increased. As we unambiguously evidenced that oxygen-functional groups are essential for high pseudocapacitance, it can be concluded that, as suggested previously [23], the capacitance reaches the maximum when an optimal ratio between the concentration of oxygen-functional groups and the conductivity is reached. When this conclusion is combined with our previous observations of the effects of specific surface area on the values of gravimetric capacitance, it can be deduced that the gravimetric capacitance can be maximized when the concentration of oxygen functional groups is finely optimized – in this way capacitance is boosted by the faradaic processes, while conductivity remains above the limit that may cause capacity loss. Similar conclusions were previously derived for carbon nanotube performance as active material in electrochemical capacitors [61]. It is also worth mentioning that, while we see the existence of a reduction potential optimal for capacitance boost of electrochemically reduced graphene-oxide, Ambrosi and Pumera [60] observed that electrocatalytic performance of electrochemically reduced graphene oxide (assessed using $[Fe(CN)_6]^{3-/4-}$ system as a probe) increases monotonically as the vertex reduction potential extends to more negative values.

Another phenomena characteristic for GO sample is gradual increase of capacitance during prolonged cycling in aqueous electrolyte. We found that the rate of the capacitance increase depends on the nature of the cation present in the electrolyte and is the lowest for Li^+ and the highest for K^+. Voltammograms shown in Fig. 10 were recorded for GO film (without any addition of Vulcan XC-72R) in 1 mol dm^{-3} aqueous LiCl before (dashed line) and after (full line) 50 potentiodynamic cycles in 1 mol dm^{-3} LiCl (A) and 1 mol dm^{-3} KCl (B). In the first case, capacitance increased by 12.8 %, while in the second case 23.8 % increase of the capacitance was observed. It is also interesting to observe that the increase of capacitive response is dominantly in the pseudocapacitive region (Section 3.2). At this point we cannot provide definite justification for observed behavior, but we suspect that this is due to the insertion of hydrated cations between graphene oxide sheets during potentiodynamic cycling. This yields a higher percentage of the surface available to the electrolyte, as well as the involvement of more oxygen functional groups in the faradaic processes.

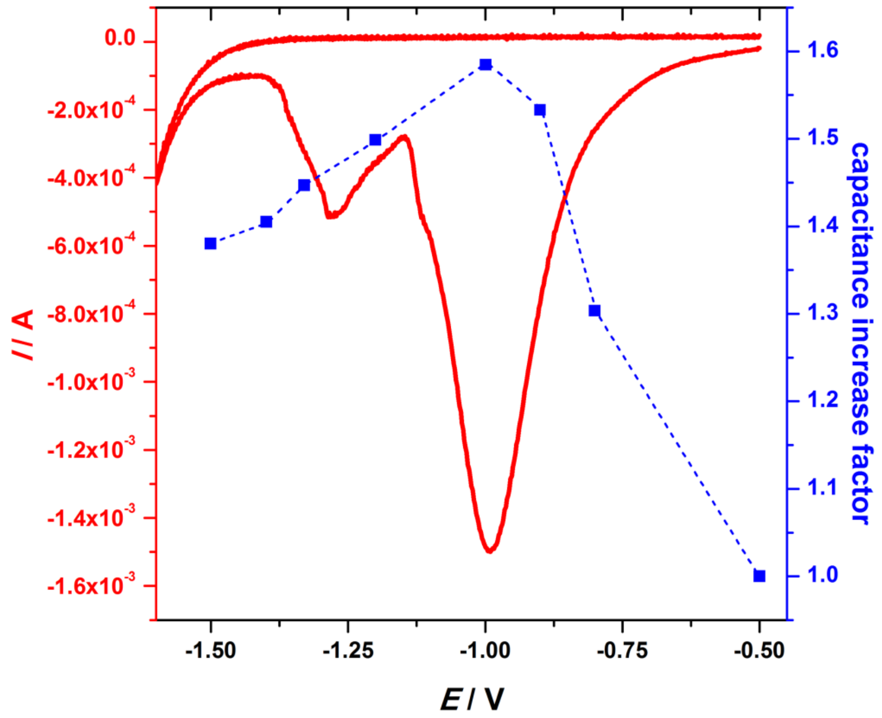

Figure 9. Thick solid line: cyclic voltammogram of graphene oxide reduction down to −1.6 V *vs*. Ag/AgCl. Squares: capacitance increase factor upon the reduction of graphene oxide to a given cathodic potential (the capacitance is measured in the potential window between −0.5 and 0.8 V vs. Ag/AgCl as for the non-reduced GO).

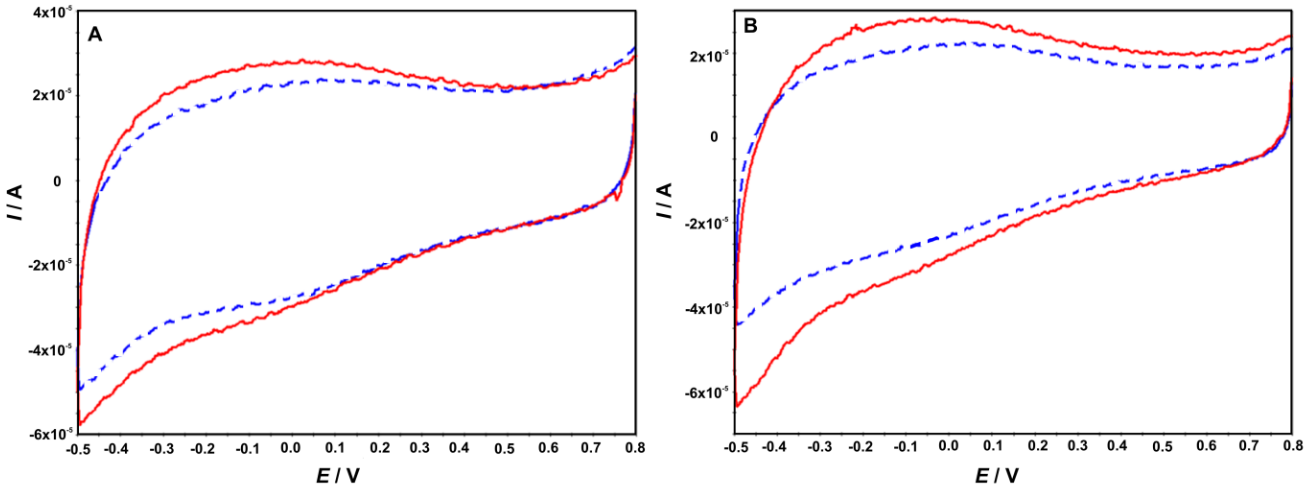

Figure 10. Cyclic voltammogram of graphene oxide recorded in 1 mol dm^{-3} aqueous LiCl before (dashed line) and after (full line) 50 cycles in 1 mol dm^{-3} LiCl (A) and 1 mol dm^{-3} KCl (B).

4. CONCLUSIONS

We have analyzed the capacitive properties of three different commercially available graphene-based materials: graphene-oxide, industrial graphene and graphene nanoplatelets, in pH-neutral alkali metal chloride solutions (LiCl, NaCl and KCl). Selected materials differ to a great extent in their specific surface area, amount of oxygen functional groups and level of structural disorder. The potential window available for capacitance measurements is limited in the case of graphene-oxide by irreversible reduction of oxygen functional groups, but for the other two materials it is almost 2 V wide. Despite the differences in their physical and chemical properties, we have observed that pseudocapacitance contributes markedly to the overall capacitance at potentials below 0.4 V *vs*. Ag/AgCl. Measured gravimetric capacitances for two materials were found to be between 19 F g^{-1} for graphene nanoplatelets and 400 F g^{-1} for industrial graphene. In general, we have observed that measured capacitance decreases as the size of cation decreases, which is especially prominent at high sweep rates in potentiodynamic investigations. The contribution of the faradaic processes increases as the concentration of oxygen functional groups increases. The DFT calculations we performed, combined with the previously published data, show unambiguously that the oxygen functional groups enhance the interactions of the functionalized graphene with alkali metal atoms (which is essentially ionic) and, consequently, their charge storage capabilities. However, the strength of the interaction critically depends on the type of alkali metal and the type of oxygen functional group. For all three materials and three electrolytes, we evaluated the limiting capacitances for both zero sweep rate (which enables all the processes that contribute to the overall capacitance) and infinite one (which enabled only fast processes of double layer charging). Using these data we observed a general relationship between the capacitance retention at high potential sweep rate and the percentage of pseudocapacitance: the capacitance retention becomes improved with the decrease of the contribution of pseudocapacitance.

The overall capacitive response depends preferentially on (i) the specific surface area and (ii) the concentration of oxygen functional groups. However, additional measurements performed with electrochemically reduced graphene oxide revealed that there is an optimal ratio between the concentration of oxygen functional groups and the conductivity, leading to a maximum capacitance. Hence, in order to achieve top capacitive performance of graphene-based materials, one should carefully optimize the concentration of oxygen functional group keeping simultaneously both specific surface area and conductivity as high as possible.

ACKNOWLEDGEMENT

This work was supported by the Serbian Ministry of Education, Science and Technological Development through the project no. III45014. A. D., N.G., I. P. and S.M. acknowledge also the financial support through the NATO Project EAP.SFPP 984925 - "DURAPEM - Novel Materials for Durable Proton Exchange Membrane Fuel Cells".

References

1. M. Inagaki, H. Konno and O. Tanaike, *J. Power Sources* 195 (2010) 7880.
2. G. Wang, L. Zhang and J. Zhang, *Chem. Soc.Rev*. 41 (2012) 797.
3. P. Simon and Y. Gogotsi, *Nat Mater* 7 (2008) 845.
4. S. Goriparti, E. Miele, F. De Angelis, E. Di Fabrizio, R. Proietti Zaccaria and C. Capiglia, *J. Power Sources* 257 (2014) 421.

5. S. H. Ha, Y. S. Jeong and Y. J. Lee, *ACS Appl. Mater. Interfaces* 5 (2013) 12295.
6. S. Gambhir, R. Jalili, D. L Officer and G. G Wallace, *NPG Asia Mater*. 7 (2015) e186.
7. P. Avouris and C. Dimitrakopoulos, *Mater. Today* 15 (2012) 86.
8. W. Lee, S. Suzuki and M. Miyayama, *Electrochim. Acta* 142 (2014) 240.
9. B. Xu, S. Yue, Z. Sui, X. Zhang, S. Hou, G. Cao and Y. Yang, *Energy Environ. Sci*. 4 (2011) 2826.
10. M. Arulepp, L. Permann, J. Leis, A. Perkson, K. Rumma, A. Jänes and E. Lust, *J. Power Sources* 133 (2004) 320
11. T. Morishita, Y. Soneda, T. Tsumura and M. Inagaki, *Carbon* 44 (2006) 2360.
12. G. Salitra, A. Soffer, L. Eliad, Y. Cohen and D. Aurbach, *J. Electrochem. Soc*. 147 (2000) 2486.
13. C. Largeot, C. Portet, J. Chmiola, P.-L. Taberna, Y. Gogotsi and P. Simon, *J. Am. Chem. Soc*. 130 (2008) 2730.
14. E. Raymundo-Piñero, K. Kierzek, J. Machnikowski and F. Béguin, *Carbon* 44 (2006) 2498.
15. C.O. Ania, V. Khomenko, E. Raymundo-Piñero, J. B. Parra and F. Béguin, *Adv. Funct. Mater*. 17 (2007) 1828.
16. D.-W. Wang, F. Li, M. Liu, G. Q. Lu and H.-M. Cheng, *J. Phys. Chem*. C 112 (2008) 9950.
17. G. Ćirić-Marjanović, I. Pašti, S. Mentus, *Prog. Mater Sci*. 69 (2015) 61.
18. Y. Li, M. van Zijll, S. Chiang and N. Pan, *J. Power Sources* 196 (2011) 6003.
19. Y.-H. Lee, K.-H. Chang and C.-C.g Hu, *J. Power Sources* 227 (2013) 300.
20. D. A. B. Iozzo, M. Tong, G. Wu and E. P. Furlani, *J. Phys. Chem.* C 119 (2015) 25235
21. L. Zhang, F. Zhang, X. Yang, G. Long, Y.g Wu, T. Zhang, K.i Leng, Y. Huang, Y. Ma, A. Yu and Y. Chen, *Sci. Rep*. 3 (2013) 1408.
22. C.-Te Hsieh, S.-M. Hsu, J.-Y. Lin and H. Teng, *J. Phys. Chem*. C 115 (2011) 12367.
23. A. S. Dobrota, I. A. Pašti and N. V. Skorodumova, *Electrochim. Acta* 176 (2015) 1092.
24. A. S. Dobrota, S. Gutić, A. Kalijadis, M. Baljozović, S. V. Mentus, N. V. Skorodumova and I. A. Pašti, *RSC Adv*. 6 (2016) 57910.
25. A. Burke, *Electrochimica Acta* 53 (2007) 1083.
26. C. O. Ania, V. Khomenko, E. Raymundo–Pinero, J. B. Parra and F. Beguin, *Adv. Funct. Mater*. 17 (2007) 1828.
27. L. Demarconnay, E. Raymundo–Piñero and F. Béguin, *Electrochem. Commun*. 2 (2010) 1275.
28. X. Yang, Y.S. He, G. Jiang, X.-Z. Liao and Z.-F. Ma, *Electrochem. Commun*. 13 (2011) 166.
29. http://www.acsmaterial.com (accessed August 8th 2016)
30. http://acsmaterial.com/product.asp?cid=26&id=1178 (accessed August 8th 2016)
31. http://www.acsmaterial.com/product.asp?cid=97&id=119 (accessed August 8th 2016)
32. http://acsmaterial.com/product.asp?cid=28&id=90 (accessed August 8th 2016)
33. U. Bogdanović, I. Pašti, G. Ćirić-Marjanović, M. Mitrić, S. P. Ahrenkiel and V. Vodnik, *ACS Appl. Mater. Interfaces* 7 (2015) 28393.
34. Y. Li, Y. Li, E. Zhu, T. McLouth, C.-Y. Chiu, X. Huang and Y Huang, *J. Am. Chem. Soc*. 134 (2012) 12326.
35. S.-M. Chen, R. Ramachandran, V. Mani and R. Saraswathi, *Int. J. Electrochem. Sci*. 9 (2014) 4072.
36. J. P. Perdew, K. Burke and M. Ernzerhof, *Phys. Rev. Lett.* 77 (1996) 3865.
37. P. Giannozzi, S. Baroni, N. Bonini, M. Calandra, R. Car, C. Cavazzoni, D. Ceresoli, G. L. Chiarotti, M. Cococcioni, I. Dabo, A. D. Corso, S. Fabris, G. Fratesi, S. de Gironcoli, R. Gebauer, U. Gerstmann, C. Gougoussis, A. Kokalj, M. Lazzeri, L. Martin-Samos, N. Marzari, F. Mauri, R. Mazzarello, S. Paolini, A. Pasquarello, L. Paulatto, C. Sbraccia, S. Scandolo, G. Sclauzero, A. P. Seitsonen, A. Smogunov, P. Umari and R. M. Wentzcovitch, *J. Phys. Condens. Matter,* 21 (2009) 395502.
38. H. J. Monkhorst and J. D. Pack, *Phys. Rev*. B, 13 (1976) 5188.
39. R. F. W. Bader, Atoms in Molecules: A Quantum Theory. Clarendon (1990), Oxford, UK.
40. G. Henkelman, A. Arnaldsson and H. Jónsson, *Comput. Mater. Sci*. 36 (2006) 354.
41. S. Grimme, *J. Comp. Chem*. 27 (2006) 1787.

42. C. Fu, G. Zhao, H. Zhang and S. Li, *Int. J. Electrochem. Sci*. 8 (2013) 6269.
43. L. Stobinski, B. Lesiak, A. Malolepszy, M. Mazurkiewicz, B. Mierzwa, J. Zemek, P. Jiricek and I. Bieloshapka, *J. Electron Spectrosc. Relat. Phenom*. 195 (2014) 145.
44. G Ćirić-Marjanović, I Pašti, N Gavrilov, A Janošević and S Mentus, *Chem. Pap*. 67 (2013) 781.
45. N. Gavrilov, I. A. Pašti, M. Mitrić, J. Travas-Sejdić, G. Ćirić-Marjanović and S. V. Mentus, *J. Power Sources* 220 (2012) 306.
46. M. Vujković, N. Gavrilov, I. Pašti, J. Krstić, J. Travas-Sejdic, G. Ćirić-Marjanović and S. Mentus, *Carbon* 64 (2013) 472.
47. A. Ganguly, S. Sharma, P. Papakonstantinou and J. Hamilton, *J. Phys. Chem*. C 115 (2011) 17009.
48. N. Ghaderi and M. Peressi, *J. Phys. Chem*. C 114 (2010) 21625.
49. P. V. Kumar, N. M. Bardhan, S. Tongay, J. Wu, A. M. Belcher and J. C. Grossman, *Nat. Chem*. 6 (2014) 151.
50. W. Yuan, Y. Zhou, Y. Li, C. Li, H. Peng, J. Zhang, Z. Liu, L. Dai and G. Shi, *Sci. Rep*. 3 (2013) 2248.
51. M. S. Goh and M. Pumera, *Electrochem. Commun*., 12 (2010) 1375.
52. N. Gavrilov, I. A. Pašti, M. Vujković, J. Travas-Sejdic, G. Ćirić-Marjanović and S. V. Mentus, *Carbon* 50 (2012) 3915.
53. A. Ambrosi, C. Kiang Chua, N. M. Latiff, A. Huiling Loo, C. H. A. Wong, A. Yong Sheng Eng, A. Bonanni and M. Pumera *Chem. Soc. Rev*. 45 (2016) 2458.
54. F. Beck, Graphite, carbonaceous materials and organic solids as active electrodes in metal-free batteries, in R. C. Alkire, H. Gerischer, D. M. Kolb and C. W. Tobias (Eds), Advances in Electrochemical Science and Engineering, Vol. 5, WILEY-VCH Verlag GmbH (2008).
55. C.-T. Hsieh and H. Teng, *Carbon* 40 (2002) 667.
56. B. Tansel, *Separ. Purif.n Technol*. 86 (2012) 119.
57. S. Farmanesh, B. G. Alamani and J. D. Rimer, *Chem. Commun*. 51 (2015) 13964.
58. H. S. Moon, J. H. Lee, S. Kwon, T. Kim and S. G. Lee, *Carbon Lett.* 16 (2015) 116.
59. D. Krepel and O. Hod, *Surf. Sci*. 605 (2011) 1633.
60. A. Ambrosi and M. Pumera, *Chem. – Eur. J.* 19 (2013) 4748.
61. Y.-T. Kim and T. Mitani, *J. Power Sources* 158 (2006) 1517.